

THE KY FAN NORMS AND BEYOND: DUAL NORMS AND COMBINATIONS FOR MATRIX OPTIMIZATION

Alexey Kravatskiy

Moscow Institute of Physics and Technology (MIPT)
kravtskii.aiu@phystech.edu

Ivan Kozyrev

Moscow Institute of Physics and Technology (MIPT)
kozyrev.in@phystech.edu

Nikolai Kozlov

Moscow Institute of Physics and Technology (MIPT)
kozlov.na@phystech.edu

Alexander Vinogradov

Moscow Institute of Physics and Technology (MIPT)
vinogradov.am@phystech.edu

Daniil Merkulov

Moscow Institute of Physics and Technology (MIPT), Skoltech, HSE, AI4Science
daniil.merkulov@phystech.edu

Ivan Oseledets

AIRI, Skoltech
i.oseledets@skoltech.ru

ABSTRACT

In this article, we explore the use of various matrix norms for optimizing functions of weight matrices, a crucial problem in training large language models. Moving beyond the spectral norm that underlies the Muon update, we leverage the duals to the Ky Fan k -norms to introduce a family of Muon-like algorithms we name *Fanions*, which happen to be similar to Dion. Then working with the duals of convex combinations of the Ky Fan k -norms and the Frobenius norm or the l_∞ norm, we construct the families of *F-Fanions* and *S-Fanions* respectively. Their most prominent members are *F-Muon* and *S-Muon*. We complement our theoretical analysis with an extensive empirical study of the algorithms across a wide range of tasks and settings, from which it follows that F-Muon and S-Muon are always on par with Muon and S-Muo, while on fine-tuning of NanoGPT and synthetic linear least squares even better than vanilla Muon.

1 INTRODUCTION

Minimizing loss functions in unprecedently high-dimensional spaces has recently become an integral and crucial part in training large language models. Hence, new scalable, time- and memory-efficient algorithms have been demanded. Besides well-known Adam (Kingma & Ba, 2014) and AdamW (Loshchilov & Hutter, 2017), recently proposed Muon (Jordan et al., 2024b) has shown promising results on training very large models (Liu et al., 2025). Its key difference from Adam and AdamW is that it has been constructed specifically for optimizing functions of weight matrices, which are common in deep learning.

That is what can be said from a practical point of view. From a theoretical perspective, a key innovation of Muon was its principled derivation of the update rule, which emerges as the solution to an optimization problem constrained by the RMS-to-RMS norm (scaled version of spectral norm) (Bernstein, 2025)

Motivated by the success of Muon, many generalizations and variations of it were proposed. Among the notable ones are Scion (Pethick et al., 2025c), Dion (Ahn et al., 2025) and Gluon (Riabinin et al., 2025). Those researches target Muon’s efficiency and establish convergence bounds. One central question, however, remains unanswered:

In deriving Muon’s update step, why constrain by the spectral norm? How would alternative norms affect performance and computational cost?

In this article, we tackle this question by first showing the connection between matrix norms and corresponding existing algorithms and discuss the theoretic bounds derived for those algorithms. We then leverage the family of norms dual to Ky Fan k-norms to derive a new class of algorithms with low-rank updates, which we call Fanions. Subsequently, we create a second, hybrid family named F-Fanions by constructing convex combinations of the Ky Fan norms with the Frobenius norm and taking dual of that composite norm. Working within the linear minimization oracle (LMO) framework we derive the explicit update formulas for both algorithm families. As it was done with Muon, we stipulate our algorithms to be fast to approximate, for which we utilize the Lanczos algorithm as described in section 5.

We then compare the performance of the algorithm families across various benchmarks (section 6):

- Synthetic least squares experiment,
- CIFAR-10 airbench,
- Pre-training NanoGPT on FineWeb dataset.

Our experiments reveal important insights about the role of matrix norms in optimization. **On a synthetic least squares problem, we observe a striking discrepancy: while some algorithms converge slowly in terms of loss, they may converge quickly in terms of gradient norm, and vice versa.** This suggests that existing theoretical guarantees may not fully explain practical algorithm performance.

Most notably, our experiments on real-world tasks demonstrate that the choice of underlying matrix norm is remarkably flexible. On CIFAR-10 airbench, properly-tuned F-Muon achieves $94.01 \pm 0.14\%$ accuracy, essentially matching Muon’s $94.00 \pm 0.13\%$ performance. On NanoGPT pre-training, F-Muon achieves 3.281 cross-entropy loss, only marginally worse than Muon’s 3.279. These results show that Muon-like algorithms can maintain competitive performance even when the underlying norm constraint is significantly modified, answering affirmatively the central question posed above. This flexibility suggests potential for developing easier-to-compute variants of successful algorithms like Muon.

2 PRELIMINARIES: LINEAR MINIMIZATION ORACLE FRAMEWORK

Training a neural network is essentially an optimization of a function of several weight matrices and a few vectors. Let us start by considering the problem of minimizing a differentiable function of a *single* matrix:

$$F(\cdot): \mathbb{R}^{m \times n} \rightarrow \mathbb{R}, \quad F(\mathbf{X}) \rightarrow \min_{\mathbf{X} \in \mathbb{R}^{m \times n}} \quad (1)$$

We equip the matrix space $\mathbb{R}^{m \times n}$ with a standard dot product $\langle \cdot, \cdot \rangle \rightarrow \mathbb{R}$ and a norm $\|\cdot\|: \mathbb{R}^{m \times n} \rightarrow \mathbb{R}_+$, which does not have to coincide with the Frobenius norm $\|\cdot\|_F$. The dual norm $\|\cdot\|^\dagger: \mathbb{R}^{m \times n} \rightarrow \mathbb{R}_+$ that is associated with $\|\cdot\|$ is defined as

$$\|\mathbf{G}\|^\dagger = \sup_{\mathbf{D} \in \mathbb{R}^{m \times n}: \|\mathbf{D}\| \leq 1} \langle \mathbf{G}, \mathbf{D} \rangle. \quad (2)$$

Such problems can be solved with an iterative algorithm based on the Linear Minimization Oracle (LMO):

$$\text{LMO}(\mathbf{M}^k) \in \arg \min_{\mathbf{D} \in \mathcal{S}} \langle \mathbf{M}^k, \mathbf{D} \rangle, \quad (3)$$

where \mathbf{M}^k is a gradient (or a momentum) of F in \mathbf{X}^k and $\mathcal{S} \subset \mathbb{R}^{m \times n}$ is some set. The update of the algorithm is defined as follows:

$$\mathbf{X}^{k+1} = \mathbf{X}^k + \gamma_k \text{LMO}(\mathbf{M}^k). \quad (4)$$

We are particularly interested in the case when \mathcal{S} is a unit ball in the norm $\|\cdot\|$:

$$\mathcal{S} = \mathcal{B}_{\|\cdot\|} = \{\mathbf{D} \in \mathbb{R}^{m \times n} \mid \|\mathbf{D}\| \leq 1\}.$$

In this case,

$$\arg \min_{\mathbf{D} \in \mathcal{S}} \langle \mathbf{M}^k, \mathbf{D} \rangle = -\{\mathbf{D} \in \mathcal{B}_1 \mid \langle \mathbf{M}^k, \mathbf{D} \rangle = \|\mathbf{M}^k\|^\dagger\},$$

and update for \mathbf{X}^k in eq. (4) simplifies to

$$\mathbf{X}^{k+1} = \mathbf{X}^k - \gamma_k \{\mathbf{D} \in \mathcal{B}_1 \mid \langle \mathbf{M}^k, \mathbf{D} \rangle = \|\mathbf{M}^k\|^\dagger\}. \quad (5)$$

Using this formula it is easy to compute updates for algorithms induced by various norms $\|\cdot\|$. For example, when the norm $\|\cdot\|$ is the Frobenius norm $\|\cdot\|_F$, eq. (5) turns into

$$\mathbf{X}^{k+1} = \mathbf{X}^k - \eta_k \frac{\mathbf{M}^k}{\|\mathbf{M}^k\|_F}, \quad (6)$$

which recovers Normalized SGD (NSGD). When one has the spectral norm $\|\cdot\|_2$, one gets

$$\mathbf{X}^{k+1} = \mathbf{X}^k - \eta_k \mathbf{U} \mathbf{V}^\top, \quad (7)$$

which is Muon without the $\sqrt{m/n}$ factor. Here, $\mathbf{M}^k = \mathbf{U} \Sigma \mathbf{V}^\top$ is the Singular Value Decomposition (SVD) of \mathbf{M}^k ($\mathbf{U} = [u_1, u_2, \dots, u_r]$, $\Sigma = \text{diag}(\sigma_1, \sigma_2, \dots, \sigma_r)$, and $\mathbf{V} = [v_1, v_2, \dots, v_r]$). Muon can be recovered by taking the RMS-to-RMS operator norm $\sqrt{\frac{n}{m}} \|\cdot\|_2$.

3 DUALS TO KY FAN NORMS INSTEAD OF THE SPECTRAL NORM

3.1 $\|\mathbf{M}^k\|_{\text{nuc}}$ AND NEON

After considering $\|\mathbf{M}^k\|_F$ and $\|\mathbf{M}^k\|_2$, it is natural to look at the nuclear norm $\|\mathbf{M}^k\|_{\text{nuc}}$.

Lemma 1. *When $\|\cdot\| = \|\cdot\|_{\text{nuc}}$, eq. (5) turns into:*

$$\mathbf{X}^{k+1} = \mathbf{X}^k - \eta_k u_1 v_1^\top \quad (8)$$

Proof. Since $\|\cdot\|^\dagger = \|\cdot\|_2$, the goal is to reach $\|\mathbf{M}^k\|_2 = \sigma_1$.

Let us note that $\Delta = u_1 v_1^\top$ delivers this value. Indeed, $\|\Delta\|_{\text{nuc}} = 1$ and by the trace property and orthogonality of the singular vectors, $\langle \mathbf{M}^k, \Delta \rangle = \langle \mathbf{U} \Sigma \mathbf{V}^\top, u_1 v_1^\top \rangle = \text{tr} \text{diag}(\sigma_1, 0, \dots, 0) = \|\mathbf{M}^k\|_2$, which completes the proof. \square

We name the derived algorithm *Neon*. In the section 5, we will discuss how to compute the Neon's update.

3.2 $\|\mathbf{M}^k\|_{\text{KF-}k}^\dagger$ AND MUON, NEON, AND CENTRALIZED DION WITHOUT ERROR FEEDBACK

Neon's and Muon's updates seem to be complete opposites: one has rank one, while the other is full-rank. It would be interesting to derive algorithms with updates of various ranks.

Schatten norms. Cesista (2025) considered Schatten- p norms $\|\mathbf{M}^k\|_{S_p} = \left(\sum_{i=1}^{\min(m,n)} \sigma_i^p \right)^{1/p}$, which produce the update:

$$\mathbf{X}^{k+1} = \mathbf{X}^k - \eta_k \mathbf{U} \frac{\text{diag}(\sigma_1^{q-1}, \dots, \sigma_{\min(m,n)}^{q-1})}{\left(\sum_{i=1}^{\min(m,n)} \sigma_i^q \right)^{\frac{q-1}{q}}} \mathbf{V}^\top$$

for $q: \frac{1}{p} + \frac{1}{q} = 1$. This formula recovers Neon when $p \rightarrow 1$ provided that $\sigma_1 > \sigma_2$, which is true on real data; NSGD when $p = 2$, and Muon when $p \rightarrow \infty$.

However, Schatten norms do not fill the gap rank: indeed, when $p > 1$, the rank of the update is full, while when $p = 1$ ($p \rightarrow 1$) it is one. Moreover, it is not clear how to calculate the update for $p \neq 1, 2, \infty$: it seems one has to know all σ_i to compute the update, which makes the problem as hard as the full SVD.

Ky Fan norms. There is another family of matrix norms, which might help us: Ky Fan norms. For $k \in \{1, \dots, \min(m, n)\}$, the Ky Fan k -norm $\|\cdot\|_{\text{KF-}k}$ is $\sum_{i=1}^k \sigma_i$, i.e. the sum of the k largest singular values of the matrix. Special cases of the Ky Fan k -norm are the Ky Fan 1-norm, which is the spectral norm, and the Ky Fan $\min\{m, n\}$ -norm, which is the nuclear norm.

Let us derive the update for an arbitrary k . Since $\|\cdot\|_{\text{KF-}k}^\dagger = \max\{\frac{1}{k} \|\cdot\|_{\text{nuc}}, \|\cdot\|_2\}$ (see Bhatia (2013), p. 96), the goal is to reach $\max\{\frac{1}{k} \sum_{i=1}^{\min(m,n)} \sigma_i, \sigma_1\}$. $\Delta = u_1 v_1^\top$ from Neon delivers σ_1 , while $\Delta = \frac{1}{k} \sum_{i=1}^{\min(m,n)} u_i v_i^\top$ from Muon (with an extra factor of $1/k$) delivers $\frac{1}{k} \sum_{i=1}^{\min(m,n)} \sigma_i$. Thus, the update is either

$$\mathbf{X}^{t+1} = \mathbf{X}^t - \eta_t u_1 v_1^\top \text{ or } \mathbf{X}^{t+1} = \mathbf{X}^t - \frac{\eta_t}{k} \mathbf{U} \mathbf{V}^\top,$$

depending on which one better minimizes the linear function $L(\mathbf{X}) \equiv F(\mathbf{X}^t) + \mathbf{M}^t (\mathbf{X} - \mathbf{X}^t)$.

The rank gap is not closed by the Ky Fan norms because the obtained update is either one-rank or full-rank.

Duals to Ky Fan norms. While Schatten norms are closed under dualization and $\|\mathbf{M}^k\|_{S_p}^\dagger = \|\mathbf{M}^k\|_{S_q}$, for Ky Fan norms it is not generally the case. $k = 1$ and $k = \min(m, n)$ are exceptional: for $k = 1$ the dual norm is $\|\cdot\|_{\text{nuc}}$ with $k = \min(m, n)$ and for $k = \min(m, n)$ the dual

norm is $\|\cdot\|_2$ with $k = 1$. For each other k , $\|\cdot\|_{\text{KF}-k} \neq \|\cdot\|_{\text{KF}-k'}$ for any k' : $k' = \min(m, n)$ and $k' = 1$ correspond to the already discussed cases, while for other k' one can change $\|\mathbf{M}^k\|_{\text{KF}-k'}$ by moving a small value between $\sigma_{k'}$ and $\sigma_{k'+1}$. During this change, $\|\mathbf{M}^k\|_2$ and $\|\mathbf{M}^k\|_{\text{nuc}}$ will remain constant, hence $\|\mathbf{M}^k\|_{\text{KF}-k}$ will not change as well.

Lemma 2. When $\|\cdot\| = \|\mathbf{M}^t\|_{\text{KF}-k}^\dagger$, eq. (5) turns into:

$$\mathbf{X}^{t+1} = \mathbf{X}^t - \eta \sum_{i=1}^k u_i v_i^\top \quad (9)$$

Proof. Since $\|\cdot\|^\dagger = \|\cdot\|_{\text{KF}-k}^{\dagger\dagger} = \|\cdot\|_{\text{KF}-k}$, the goal to reach $\|\mathbf{M}^t\|_{\text{KF}-k}$.

Let us note that $\Delta = \sum_{i=1}^k u_i v_i^\top$ delivers the value. Indeed, $\langle \mathbf{M}^t, \Delta \rangle = \langle \mathbf{U} \Sigma \mathbf{V}^\top, \sum_{i=1}^k u_i v_i^\top \rangle = \sum_{i,j=1}^{r,k} \langle u_i \sigma_i v_i^\top, u_j v_j^\top \rangle = \sum_{i=1}^k \sigma_i = \|\mathbf{M}^t\|_{\text{KF}-k}$, which completes the proof. \square

These updates constitute a family *Fanions*, LMO-based algorithms under the $\|\mathbf{M}^t\|_{\text{KF}-k}^\dagger$ norms. The algorithm for a particular k we will call *Fanion- k* . Thus, Muon is a Fanion-min{ m, n }, while Neon is a Fanion-1. Moreover, the unsharded version of the rank- r Dion (Algorithm 1 from Ahn et al. (2025)) without the error feedback and without scaling of the update is actually a Fanion- r (see Pethick (2025), where Dion is written down in a notation more similar to ours).

4 CONIC COMBINATION OF LMO-ALGORITHMS IS AN LMO-ALGORITHM

Simply applying norm dual to the Ky Fank k -norm however, is not enough to provide family of algorithms diverse enough for our cause. Next we consider linear combinations of algorithms from LMO framework, which happen to be LMO-algorithms too, as we show in succeeding paragraphs.

4.1 GENERAL CASE

First, we need a well-known fact mentioned, for example, in Yu (2012, Table 1). For the sake of completeness, we provide a proof here.

Lemma 3. Let $\|\cdot\|_{(1)}, \dots, \|\cdot\|_{(n)}$ be norms on a finite-dimensional Euclidean space, and let $\alpha_1, \dots, \alpha_n$ be non-negative reals. Define

$$\|x\| := \sum_{i=1}^n \alpha_i \|x\|_{(i)}.$$

Then the dual unit ball of $\|\cdot\|$ satisfies

$$\mathcal{B}_{\|\cdot\|^\dagger} = \sum_{i=1}^n \alpha_i \mathcal{B}_{\|\cdot\|_{(i)}^\dagger}$$

where \sum denotes the Minkowski sum and $\mathcal{B}_{\|\cdot\|_{(i)}^\dagger}$ is the unit ball of the dual norm $\|\cdot\|_{(i)}^\dagger$.

Proof. Let us first prove the lemma for the case $n = 2$. Denote $f(x) = \alpha_1 \|x\|_{(1)}$ and $g(x) = \alpha_2 \|x\|_{(2)}$, such that $\|x\| = f(x) + g(x)$. Recall two standard facts:

1. For any norm $\|\cdot\|$ and $\lambda > 0$,

$$(\lambda\|\cdot\|)^*(y) = \sup_x (\langle y, x \rangle - \lambda\|x\|) = \delta_{\lambda\mathcal{B}_{\|\cdot\|^{\dagger}}}(y),$$

i.e., the indicator function of the scaled dual ball.

2. The Fenchel conjugate of a sum satisfies

$$(f + g)^*(y) = \inf_{u+v=y} (f^*(u) + g^*(v)).$$

Applying these to f and g , we have

$$f^*(u) = \delta_{\alpha_1\mathcal{B}_{\|\cdot\|_{(1)}^{\dagger}}}(u), \quad g^*(v) = \delta_{\alpha_2\mathcal{B}_{\|\cdot\|_{(2)}^{\dagger}}}(v).$$

Thus,

$$\|\cdot\|^*(y) = (f + g)^*(y) = \inf_{u+v=y} (\delta_{\alpha_1\mathcal{B}_{\|\cdot\|_{(1)}^{\dagger}}}(u) + \delta_{\alpha_2\mathcal{B}_{\|\cdot\|_{(2)}^{\dagger}}}(v)) = \delta_{\alpha_1\mathcal{B}_{\|\cdot\|_{(1)}^{\dagger}} + \alpha_2\mathcal{B}_{\|\cdot\|_{(2)}^{\dagger}}}(y).$$

By definition, the conjugate of a norm is exactly the indicator of its dual unit ball:

$$\|\cdot\|^*(y) = \delta_{\mathcal{B}_{\|\cdot\|^{\dagger}}}(y).$$

Therefore, $\mathcal{B}_{\|\cdot\|^{\dagger}} = \alpha_1\mathcal{B}_{\|\cdot\|_{(1)}^{\dagger}} + \alpha_2\mathcal{B}_{\|\cdot\|_{(2)}^{\dagger}}$.

Now we prove the general case by induction. The base case ($n = 2$) is already proven. Suppose that the assumption of the lemma holds for $n = k$. Then, for $n = k + 1$,

$$\|x\| = \sum_{i=1}^k \alpha_i \|x\|_{(i)} + \alpha_{k+1} \|x\|_{(k+1)} = \|x\|_{(1:k)} + \alpha_{k+1} \|x\|_{(k+1)}.$$

Applying the result for $n = 2$ combined with the induction assumption, we obtain

$$\mathcal{B}_{\|\cdot\|^{\dagger}} = \mathcal{B}_{\|\cdot\|_{(1:k)}^{\dagger}} + \alpha_{k+1}\mathcal{B}_{\|\cdot\|_{(k+1)}^{\dagger}} = \sum_{i=1}^{k+1} \alpha_i \mathcal{B}_{\|\cdot\|_{(i)}^{\dagger}},$$

which proves the lemma. \square

Lemma 4. *Let $\|\cdot\|_{(1)}, \dots, \|\cdot\|_{(n)}$ be norms on a finite-dimensional Euclidean space, and let $\alpha_1, \dots, \alpha_n$ be non-negative reals. Consider Linear Minimization Oracles $\text{LMO}_1, \dots, \text{LMO}_n$, corresponding to the unit balls of these norms. Then, $\sum_{i=1}^n \alpha_i \text{LMO}_i$ is the LMO corresponding to the norm $\|\cdot\|$ dual to the $\sum_{i=1}^n \alpha_i \|\cdot\|_{(i)}^{\dagger}$.*

Proof. Using lemma 3 and the fact $\|\cdot\|^{\dagger\dagger} = \|\cdot\|$, we can obtain general form of the unit ball in the $\|\cdot\|$ norm: $\mathcal{B}_{\|\cdot\|} = \sum_{i=1}^n \alpha_i \mathcal{B}_{\|\cdot\|_{(i)}}$. Thus, the linear function minimization objective on a $\|\cdot\|$ norm ball can be transformed as follows:

$$\arg \min_{\mathbf{D} \in \mathcal{B}_{\|\cdot\|}} \langle \mathbf{M}, \mathbf{D} \rangle = \arg \min_{\mathbf{D}_1 \in \alpha_1 \mathcal{B}_{\|\cdot\|_{(1)}}, \dots, \mathbf{D}_n \in \alpha_n \mathcal{B}_{\|\cdot\|_{(n)}}} \langle \mathbf{M}, \sum_{i=1}^n \mathbf{D}_i \rangle = \sum_{i=1}^n \arg \min_{\mathbf{D}_i \in \mathcal{B}_{\|\cdot\|_{(i)}}} \langle \mathbf{M}, \mathbf{D}_i \rangle,$$

where the last summation denotes the Minkowski sum. This immediately implies $\sum_{i=1}^n \alpha_i \text{LMO}_i \in \arg \min_{\mathbf{D} \in \mathcal{B}_{\|\cdot\|}} \langle \mathbf{M}, \mathbf{D} \rangle$, which proves the claim of the lemma. \square

Applying it to optimization algorithms we obtain the following corollary.

Corollary 1. *Let there be a finite family of LMO based algorithms indexed by $i = 1, \dots, n$, where the update of the i -th algorithm is defined by*

$$\mathbf{X}^{k+1} - \mathbf{X}^k = \gamma_k \text{LMO}_i(\mathbf{M}^k),$$

and LMO_i corresponds to the unit ball of norm $\|\cdot\|_i$. For arbitrary non-negative $\alpha_1, \dots, \alpha_n$, the algorithm with the update given by

$$\mathbf{X}^{k+1} - \mathbf{X}^k = \gamma_k \sum_{i=1}^n \alpha_i \text{LMO}_{\|\cdot\|_{(i)}}(\mathbf{M}^k)$$

is an LMO-algorithm itself, with LMO corresponding to the unit ball of the norm $\|\cdot\|$ dual to the norm given by $\sum_{i=1}^n \alpha_i \|\cdot\|_{(i)}^\dagger$.

4.2 FROBENIUSIZE THEM: F-MUON AND F-NEON

Let us construct the concrete examples of algorithms given by linear combinations of LMO-algorithms. It follows from corollary 1 that those algorithms can also be viewed as LMO-algorithms.

Combining Fanions- k with another excellent LMO-algorithm, NSGD, we obtain the family of algorithms with updates defined by

$$\mathbf{X}^{t+1} = \mathbf{X}^t - \gamma \left(\alpha \sum_{i=1}^k u_i v_i^\top + (1 - \alpha) \frac{\mathbf{M}^k}{\|\mathbf{M}^k\|_F} \right). \quad (10)$$

By corollary 1, this is an LMO-algorithm corresponding to the unit ball of the norm $\|\cdot\|_{F-KF-k}$, given by

$$\|\cdot\|_{F-KF-k}^\dagger = \alpha \|\cdot\|_{KF-k}^\dagger + (1 - \alpha) \|\cdot\|_F^\dagger. \quad (11)$$

We name the derived algorithms *F-Fanions*. A bit of information and visualizations related to the $\|\cdot\|_{F*}$ norm is presented in the appendix (see eq. (14), fig. 5a).

Two edge members of this family, with $k = 1$ and $k = \min\{m, n\}$ correspondingly, are *F-Neon* and *F-Muon*.

4.3 ADD SIGNSGD: S-MUON AND S-NEON

Trivial formulas, but we need more experiments.

5 COMPUTING THE UPDATES

We employ the thick-restarted Lanczos method for the symmetric eigenvalue problem (thick-restart Lanczos, TRLan) to compute the low-rank updates of Fanions. We apply TRLan to either $\mathbf{M}^{k\dagger} \mathbf{M}^k$ or $\mathbf{M}^k \mathbf{M}^{k\dagger}$ (whichever matrix is smaller). We use the CuPy implementation of `cupy.sparse.linalg.svds` (Preferred Infrastructure & Developers, 2025) which internally relies on TRLan (Simonz, 1998).

TRLan is specifically designed for efficiently approximating the largest singular values and corresponding singular vectors of very large matrices. The thick-restart strategy retains the

most informative Ritz vectors across restarts, which dramatically accelerates convergence while keeping memory consumption moderate. TRLan is particularly attractive in our GPU setting because its dominant cost is a modest number of highly parallelizable matrix-vector multiplications (matvecs) and it avoids full reorthogonalization against the entire Krylov basis by using short recurrence relations combined with thick restarting.

The per-cycle complexity is $\mathcal{O}(mn^2 + n^2k + nk^2)$, where $m \geq n$ are the dimensions of the target matrix and k is the size of the retained subspace (typically $k \ll n$).

In Table 1, we compare TRLan against randomized SVD (RSVD) and simple power iterations when computing the rank- k update used in Fanion- k and related algorithms. Experiments are performed on dense random matrices with i.i.d. $\mathcal{N}(0, 1)$ entries and use CPU implementations for fair comparison. We report:

- err_1 : relative error in the Frobenius norm of $\sum_i^k u_i v_i^T$,
- err_2 : relative error in the Frobenius norm of $\sum_i^k \sigma_i u_i v_i^T$.

On 500×500 matrices, TRLan and RSVD require comparable wall-clock time, but TRLan delivers orders-of-magnitude lower error and far fewer matvecs. On larger 5000×5000 matrices the advantage becomes even more pronounced: TRLan is 3-4 times faster than RSVD while using ~ 30 times fewer matvecs at comparable or better accuracy.

An interesting empirical observation is that RSVD tends to approximate the *singular values* themselves reasonably well but the reconstructed low-rank matrix noticeably deviates from the truncated SVD, whereas TRLan provides an excellent approximation to the truncated SVD matrix itself (low err_2) at the cost of occasionally less accurate individual singular values. This makes TRLan the preferred choice for algorithms like Neon/Fanion- k that only need the low-rank term $\sum_i \sigma_i u_i v_i^\top$, but less ideal for methods (e.g., Dion) that explicitly require accurate σ_i for error feedback or step-size control.

A current practical limitation is the lack of a native PyTorch implementation of thick-restart Lanczos; existing PyTorch-based randomized SVD routines cannot match TRLan's accuracy/efficiency combination for the matrix reconstruction task.

For reference, Table 2 shows results for the Newton-Schulz polar decomposition iteration on the same matrices, err_1 is the relative error of UV^T (29-30 iterations to converge, significantly higher matvec count than TRLan).

Matrix sizes	k	Method	Time (s)	Matvecs	Iterations	err_1	err_2
500×500	5	Power Iterations	0.062	2005	200	$9.2 \cdot 10^{-3}$	$9.1 \cdot 10^{-3}$
500×500	5	RSVD	0.017	1170	38	$9.8 \cdot 10^{-3}$	$9.6 \cdot 10^{-3}$
500×500	5	TRLan	0.018	131	65	$9.6 \cdot 10^{-5}$	$9.4 \cdot 10^{-5}$
500×500	50	Power Iterations	0.44	43750	437	$9.9 \cdot 10^{-3}$	$9.0 \cdot 10^{-3}$
500×500	50	RSVD	0.61	6120	50	$9.9 \cdot 10^{-3}$	$9.1 \cdot 10^{-3}$
500×500	50	TRLan	0.16	462	231	$3.3 \cdot 10^{-7}$	$3.0 \cdot 10^{-7}$
5000×5000	5	Power Iterations	9.6	9065	906	$8.6 \cdot 10^{-3}$	$8.6 \cdot 10^{-3}$
5000×5000	5	RSVD	2.1	5640	187	$9.7 \cdot 10^{-3}$	$9.7 \cdot 10^{-3}$
5000×5000	5	TRLan	0.70	205	102	$7.7 \cdot 10^{-3}$	$7.7 \cdot 10^{-3}$

Table 1: Comparison of methods for computing rank- k updates on dense random matrices (CPU, double precision). Lower is better in all columns.

Matrix size	Time (s)	Matvecs	Iterations	err_1
500×500	0.041	27 000	27	4.8e-3
5000×5000	26.4	290 000	29	6.5e-3

Table 2: Newton–Schulz iteration on the same matrices (for reference).

6 EXPERIMENTS

6.1 RANDOMIZED LINEAR LEAST SQUARES

First, we compare F-Fanions on the following convex L-smooth problem:

$$F(\mathbf{X}) = \frac{1}{2} \langle (\mathbf{X} - \mathbf{S}), \mathbf{M}(\mathbf{X} - \mathbf{S})\mathbf{N} \rangle \rightarrow \min_{\mathbf{X} \in \mathbb{R}^{m \times n}} \quad (12)$$

where $\mathbf{X} \in \mathbb{R}^{m \times n}$, $m = 500$ and $n = 500$ are typical dimensions of a neural network weight matrix, $\mathbf{S} \in \mathbb{R}^{m \times n}$, $\mathbf{M} \in \mathbb{S}_+^m$ and $\mathbf{N} \in \mathbb{S}_+^n$ are positive-semidefinite matrices. The spectra of \mathbf{M} and \mathbf{N} are uniformly distributed in the $(0, 1)$ interval. We set $\mathbf{S} = 0$, and $\mathbf{X}^0 \sim 0.1\mathcal{N}(0, \mathbf{I})$.

We run different Fanions and their respective F-Fanions with $\alpha = 1/2$: Neon (Fanion-1), Fanion-2, Fanion-5, Fanion-100, and Muon (Fanion-500). Also, we test S-Fanions with $\alpha = 1/2$ and `sign_lr_coeff=0.01`. We test them against Normalized SGD and SignSGD, which are also F-Fanion and S-Fanion respectively with $\alpha = 0$ and an arbitrary k .

Since theoretical bounds (Kovalev, 2025; Riabinin et al., 2025) rely on a very loose norm bound $\|\cdot\| \leq \rho\|\cdot\|_F$, we do not derive learning rate or momentum from the smoothness constants that also depend on the norm choice. Rather, we find such `(lr, momentum)` pair that the loss threshold 0.01 is reached in a minimal number of iterations. This setting is the most realistic, and at the same time aligns with the corollaries of the convergence theorems where constant learning rate and momentum coefficients are proposed.

The results are presented in fig. 1 and section D.

Both F-Muon and S-Muon converge faster and to a lower loss and a lower Frobenius norm of the gradient than NSGD, Muon, or SignSGD.

6.2 CIFAR-10 AIRBENCH

We compare the algorithms on the CIFAR-10 airbench (Keller, 2023). First, to test the impact of α , we run F-Muon for different α with the same `lr=0.24(1 - step/total_steps)`, `momentum=0.6`, `nesterov=True` and weight normalization, as have been finetuned by Keller Jordan, 10 repetitions for each α . We record the accuracy after 8 epochs of training (fig. 2a).

Then we tune F-Muon with $\alpha = 0.5$. Tuned parameters are `lr=0.4(1 - step/total_steps)`, `momentum=0.65`, `nesterov = True`. Tuned F-Muon reaches $94.01 \pm 0.14\%$ after 8 epochs (averaged by 200 iterations), matching Muon’s accuracy and variance. Once again we measure `val_accuracy`(α) curve (fig. 2b). We notice that even when $\alpha = 0.1$, the accuracy is much higher than in the case of vanilla NSGD.

We tune S-Muon with $\alpha = 0.5$ for the best `(lr, momentum, sign_lr_coeff)` and by setting `lr=0.42(1 - step/total_steps)`, `momentum=0.65`, `nesterov =`

Table 3: lmo optimizers in Schatten S_p norms and in l_p norms. g is the gradient. When it is a matrix, $g = \mathbf{U}\Sigma\mathbf{V}^\top$

Method	lmo constraint set \mathcal{D}	lmo	Reference
Normalized SGD	l_2 -ball, S_2 -ball	$-\eta \frac{g}{\ g\ _2} = -\eta \frac{g}{\ g\ _F}$	(Hazan et al., 2015)
Momentum Normalized SGD	Ball in l_2 , or Ball in S_2	$-\eta \frac{g}{\ g\ _2} = -\eta \frac{g}{\ g\ _F}$	(Cutkosky et al., 2020)
SignSGD	Ball in Max-norm l_∞	$-\eta \text{sign}(g)$	(Bernstein et al., 2018, Thm. 1)
Signum	Ball in Max-norm l_∞	$-\eta \text{sign}(g)$	(Bernstein et al., 2018, Thm. 3)
Muon	Ball in Spectral S_∞	$-\eta \bar{U} \bar{V}^\top$	(Jordan et al., 2024b)
Gauss-Southwell Coordinate Descent	Ball in l_1	$-\eta \sum_{i \in \arg \max g_i^t } \text{sign}(g_i^t) e_i$	(Shi et al., 2016, p. 19)
Neon	Ball in Nuclear S_1	$-\eta u_1 v_1^\top$	This work

True, `sign_lr_coeff = 0.003` get **94.02 ± 0.13%**, which is even higher than for vanilla Muon.

The Muon-level performance is surprising for the contorted geometry of F-Muon and S-Muon. F-Muon can be visualized by fig. 3, where the LMO balls of Muon and F-Muon for real lr are plotted in a 2D space of singular values. S-Muon cannot be visualized because the l_∞ norm is not a function of singular values, while $\|\cdot\|_2$, when plotted for the $\mathbb{R}^{m \times n}$ space with $m, n > 2$, requires at least a 4D space. However, it is plain that the LMO ball of S-Muon significantly differs from the ball of Muon because the $lr(1 - \alpha)\text{sign_lr_coeff} = 6.3 \times 10^{-4}$, which is comparable to the usual lr of SignSGD for deep learning problems.

The most pathological case is $\alpha > 1$, which corresponds to the LMO with an area that is not a norm ball! Despite this violation, the mixture of algorithms reaches almost the same accuracy as vanilla Muon.

These observations raise the question of how much LMO-based algorithms are sensitive to the constraint area.

6.3 NANO GPT SPEEDRUN

We test F-Muon on the NanoGPT speedrun (Jordan et al., 2024a). For $\alpha = 0.5$, the optimal parameters are $lr=0.07$, $momentum=0.95$, while for Muon they were $lr=0.05$, $momentum=0.95$. After testing for 1750 steps we get 3.281 cross-entropy loss. For Muon, it falls below the target threshold 3.28 and reaches 3.279. However, this difference is negligible if one looks at fig. 4. It is even more striking, considering the fact that this F-Muon is an average of Muon and NSGD, and the latter performed quite poorly.

Again, as on the CIFAR airbench, if we set $\alpha = -0.1$ that corresponds to no ball, we get a 3.2818 loss, which is a small difference from the baseline.

7 ALGORITHMS FOR VECTORS → ALGORITHMS FOR MATRICES

One cannot but notice the similarity between the updates LMO optimizers in the vector l_p and the matrix Schatten S_p norms, which is illustrated by table 3. However, the parallels are not limited to this similarity and can be traced even in the empirical observations. SignSGD is very close to Adam, as noted in Bernstein & Newhouse (2024), and both Adam and Muon perform well in training large models. NSGD is the same for both matrix and vector cases. Greedy Coordinate Descent is not applied to high-dimensional problems, so from this perspective it is not surprising that one-rank Neon underperforms on such problems.

8 RELATED WORK AND DISCUSSION

Since Muon (Jordan et al., 2024b) is a very successful and popular optimizer for functions of weight matrices, a lot of research has been put into, first, further improving its performance and, second, explaining its success.

Improvements of Muon. Regarding the first point, a large number of applications and improvements of Muon have been proposed in less than a year. Liu et al. (2025) adapted the algorithm for training language models larger than NanoGPT. Shah et al. (2025) organized efficient hyperparameter transfer by combining Muon with maximal update parametrization. To construct their COSMOS optimizer, Chen et al. (2025) applied computationally intensive updates of SOAP optimizer (Vyas et al., 2025) to a low-dimensional "leading eigensubspace" while using memory-efficient methods like Muon for the remaining parameters. Amsel et al. (2025); Grishina et al. (2025) proposed more efficient alternatives to Newton-Schulz algorithm. Si et al. (2025) introduced AdaMuon which combines element-wise adaptivity with orthogonal updates. We suppose that the described above or similar techniques can be applied to our optimizers as well. For example, F-Muon and S-Muon also benefit from faster alternatives to Newton-Schulz iterations, and Fanions may be a great substitute to Muon in COSMOS, because, as we have shown in Section 5, Lanczos algorithm is much faster than Newton-Schulz iterations on very large matrices.

Theory behind Muon. Regarding the second point, there has been a prolonged gap in theory behind Muon, simplistic derivation of Bernstein (2025) based on Bernstein & Newhouse (2024) excluded. This gap, as it seems to us, is not even now completely closed. For example, Kovalev (2025) has provided convergence guarantees of Muon and in various settings, from which, however, Muon's supremacy cannot be recovered. Indeed, although the obtained bounds depend on the norm choice, the asymptotics of the convergence remain the same as for NSGD and other optimizers, $K = \mathcal{O}(\varepsilon^{-4})$ in an L-smooth stochastic case.

A similar drawback has the article Riabinin et al. (2025), where L-smoothness assumption is replaced with a more practical (L_0, L_1) -smoothness. By estimating smoothness and substituting it into their Theorem 1, the authors recovered the optimal fine-tuned stepsizes reported by Pethick et al. (2025c). However, they have not showed the optimality of the spectral or the RMS-to-RMS norm, which is observed in practice, as our comparison with NSGD highlights.

Common important drawback of the analyses is the consideration of the convergence by the norm of the gradient. As we showed in our experiments on CIFAR, the gradient norm may decrease only by a factor of ten, when the accuracy reaches 100%.

We suppose that the reason for the recorded stark discrepancy between Neon and Muon performance, both of which are described by Stochastic Conditional Gradient (Pethick et al., 2025c) or Gluon frameworks, lies in the structure of the norm ball or in the preconditioner interpretation (Pethick et al., 2025a), which must be an object of further research.

The LMO and Error Feedback. We already mentioned that rank- k unsharded Dion without error feedback and scaling of the update is Fanion- k . Since error feedback for Dion is very important as discovered by the ablation study in Ahn et al. (2025), F-Fanions and S-Fanions will benefit from it as well. In the context of federated learning, error feedback is effective even for compressed Muon (Gruntkowska et al., 2025a). The advantage of Fanions and S-Fanions is that less bits are required for transmission: $\sum_{i=1}^k u_i v_i^\top$ is easily transmitted as $\{u_1, v_1, \dots, u_k, v_k\}$ $((m+n) \times k$ floats), while the sign part is as usual coded in $m \times n$ bits. Thus, the compression is "built-in". Moreover, there is an intriguing possibility to construct differentially private

Fanions and S-Fanions with the specific more optimal non-Gaussian noise, as was done with DP-signSGD (Jang et al., 2024). This we leave for future research.

The nuclear norm in the LMO. As we found out only when transforming our results into an article, the nuclear norm has already been explored in the context of the linear minimization oracle. Pethick et al. (2025b) applied it to create ν SAM, a new sharpness-aware minimization technique. It would be interesting to substitute $\|\cdot\|_{\text{nuc}}$ with $\|\cdot\|_{\text{KF}-k}^\dagger$ in their approach. Since the SAM-neighborhood becomes more diverse, $k > 1$ might add to the accuracy boost, while preserving a small memory footprint and a small time overhead, if Dion-style power iterations are used.

Orthogonal research. Fanions, F-Fanions, and S-Fanions benefit from the general theoretical description of Riabinin et al. (2025), and better learning rates can be predicted by calculating the trajectory smoothness. They could be transformed to Drop-Fanions by updating only some layers as in Gruntkowska et al. (2025b). They could be viewed as approximations of the Non-Euclidean Broximal Point Method for the corresponding norms (Gruntkowska & Richtárik, 2025). One can clip them to produce ClippedScion-like algorithms (Pethick et al., 2025d). They could be made more memory-effective by the zero-order techniques that worked for Muon (Petrov et al., 2025). Finally, the results from Shulgin et al. (2025) can be used to explain the robustness of Muon to the norm change that occurred in our experiments and to theoretically derive faster yet working approximate schemes to calculate the LMO; power iterations with a very limited number of iterations is a good algorithm to consider for the analysis.

9 CONCLUSION

In this article, we have generalized several successful algorithms, like Muon and Dion, to the lmo-based algorithms in the $\|\cdot\|_{\text{KF}-k}^\dagger$ norm. Also we have proposed the technique of “regularizing” the updates with NSGD, a trick to increase the robustness of the algorithms, which is motivated by the consideration of the $\|\cdot\|_{F_*}$, $\|\cdot\|_{F_2}$, and general $\|\cdot\|_{F-\text{KF}-k}$ norms. Generalizations of well-known norms and subsequent combinations of them may further improve performance of lmo-based algorithms. If a theory is developed that explains the discrepancy between performance of different algorithms based on the matrix norms, one will probably be able to intentionally construct norms optimal to given architectures and probably even their parameters.

We suggest that future works that deal with the non-Euclidean LMO explain in corollaries to their convergence theorems the empirical superiority of Muon to other Fanions. Without that, it is hard to believe that the bounds are relevant for practitioners.

10 AUTHOR CONTRIBUTIONS

IO suggested using the nuclear norm in the Bernstein & Newhouse (2024) framework. DM supervised the project and helped with editing the article. IK suggested using composite norms (though not the ones that induce F-Fanions and S-Fanions) and refactored section 4. NK suggested Lanczos algorithm as the most precise means to compute Fanions’ updates, conducted experiments to prove it, and wrote section 5. AV tested Neon on the finetuning of NanoGPT on Tiny Stories. All other work was done by AK.

REFERENCES

- Kwangjun Ahn, Byron Xu, Natalie Abreu, Ying Fan, Gagik Magakyan, Pratyusha Sharma, Zheng Zhan, and John Langford. Dion: Distributed orthonormalized updates, 2025. URL <https://arxiv.org/abs/2504.05295>.
- Noah Amsel, David Persson, Christopher Musco, and Robert M Gower. The polar express: Optimal matrix sign methods and their application to the muon algorithm. *arXiv preprint arXiv:2505.16932*, 2025.
- Jeremy Bernstein. Deriving muon, 2025. URL <https://jeremybernste.in/writing/deriving-muon>.
- Jeremy Bernstein and Laker Newhouse. Old optimizer, new norm: An anthology. *arXiv preprint arXiv:2409.20325*, 2024.
- Jeremy Bernstein, Yu-Xiang Wang, Kamyar Azizzadenesheli, and Animashree Anandkumar. signsdg: Compressed optimisation for non-convex problems. In *International conference on machine learning*, pp. 560–569. PMLR, 2018.
- Rajendra Bhatia. *Matrix analysis*, volume 169. Springer Science & Business Media, 2013.
- Franz Louis Cesista. Steepest Descent under Schatten-p Norms, February 2025. URL <https://leloykun.github.io/ponder/steepest-descent-schatten-p/>.
- Weizhu Chen, Chen Liang, Tuo Zhao, Zixuan Zhang, Hao Kang, Liming Liu, Zichong Li, and Zhenghao Xu. Cosmos: A hybrid adaptive optimizer for memory-efficient training of llms, 2025. URL <https://arxiv.org/abs/2502.17410>.
- Ashok Cutkosky, Harsh Mehta, and Francesco Orabona. Momentum-based variance reduction in nonconvex sgd. *Advances in Neural Information Processing Systems*, 2020.
- Ekaterina Grishina, Matvey Smirnov, and Maxim Rakhuba. Accelerating newton-schulz iteration for orthogonalization via chebyshev-type polynomials, 2025. URL <https://arxiv.org/abs/2506.10935>.
- Kaja Gruntkowska and Peter Richtárik. Non-euclidean proximal point method: A blueprint for geometry-aware optimization, 2025. URL <https://arxiv.org/abs/2510.00823>.
- Kaja Gruntkowska, Alexander Gaponov, Zhirayr Tovmasyan, and Peter Richtárik. Error feedback for muon and friends, 2025a. URL <https://arxiv.org/abs/2510.00643>.
- Kaja Gruntkowska, Yassine Maziane, Zheng Qu, and Peter Richtárik. Drop-muon: Update less, converge faster, 2025b. URL <https://arxiv.org/abs/2510.02239>.
- Elad Hazan, Kfir Levy, and Shai Shalev-Shwartz. Beyond convexity: Stochastic quasi-convex optimization. *Advances in neural information processing systems*, 28, 2015.
- Jonggyu Jang, Seongjin Hwang, and Hyun Jong Yang. Rethinking DP-SGD in discrete domain: Exploring logistic distribution in the realm of signSGD. In Ruslan Salakhutdinov, Zico Kolter, Katherine Heller, Adrian Weller, Nuria Oliver, Jonathan Scarlett, and Felix Berkenkamp (eds.), *Proceedings of the 41st International Conference on Machine Learning*, volume 235 of *Proceedings of Machine Learning Research*, pp. 21241–21265. PMLR, 21–27 Jul 2024. URL <https://proceedings.mlr.press/v235/jang24a.html>.

Keller Jordan, Jeremy Bernstein, Brendan Rappazzo, @fernbear.bsky.social, Boza Vlado, You Jiacheng, Franz Cesista, Braden Koszarsky, and @Grad62304977. modded-nanopt: Speedrunning the nanopt baseline, 2024a. URL <https://github.com/KellerJordan/modded-nanopt>.

Keller Jordan, Yuchen Jin, Vlado Boza, Jiacheng You, Franz Cesista, Laker Newhouse, and Jeremy Bernstein. Muon: An optimizer for hidden layers in neural networks, 2024b. URL <https://kellerjordan.github.io/posts/muon/>.

Jordan Keller. cifar10-airbench, 2023. URL <https://github.com/KellerJordan/cifar10-airbench>.

Diederik P Kingma and Jimmy Ba. Adam: A method for stochastic optimization. *arXiv preprint arXiv:1412.6980*, 2014.

Dmitry Kovalev. Understanding gradient orthogonalization for deep learning via non-euclidean trust-region optimization. *arXiv preprint arXiv:2503.12645*, 2025.

Jingyuan Liu, Jianlin Su, Xingcheng Yao, Zhejun Jiang, Guokun Lai, Yulun Du, Yidao Qin, Weixin Xu, Enzhe Lu, Junjie Yan, et al. Muon is scalable for llm training. *arXiv preprint arXiv:2502.16982*, 2025.

Ilya Loshchilov and Frank Hutter. Decoupled weight decay regularization. *arXiv preprint arXiv:1711.05101*, 2017.

Thomas Pethick. Understanding dion, 2025. URL <https://pethick.dk/posts/2025-08-18-understanding-dion/>.

Thomas Pethick, Kimon Antonakopoulos, Antonio Silveti-Falls, Leena Chennuru Vankadara, and Volkan Cevher. Training neural networks at any scale, 2025a. URL <https://arxiv.org/abs/2511.11163>.

Thomas Pethick, Parameswaran Raman, Lenon Minorics, Mingyi Hong, Shoham Sabach, and Volkan Cevher. ν SAM: Memory-efficient sharpness-aware minimization via nuclear norm constraints. *Transactions on Machine Learning Research*, 2025b. ISSN 2835-8856. URL <https://openreview.net/forum?id=V6ia5hWIMD>.

Thomas Pethick, Wanyun Xie, Kimon Antonakopoulos, Zhenyu Zhu, Antonio Silveti-Falls, and Volkan Cevher. Training deep learning models with norm-constrained lmos. *arXiv preprint arXiv:2502.07529*, 2025c.

Thomas Pethick, Wanyun Xie, Mete Erdogan, Kimon Antonakopoulos, Tony Silveti-Falls, and Volkan Cevher. Generalized gradient norm clipping & non-euclidean (l_0, l_1) -smoothness, 2025d. URL <https://arxiv.org/abs/2506.01913>.

Egor Petrov, Grigoriy Evseev, Aleksey Antonov, Andrey Veprikov, Nikolay Bushkov, Stanislav Moiseev, and Aleksandr Beznosikov. Leveraging coordinate momentum in signs gd and muon: Memory-optimized zero-order, 2025. URL <https://arxiv.org/abs/2506.04430>.

Inc. Preferred Infrastructure and CuPy Developers. CuPy: cupyx.scipy.sparse.linalg.svds — api reference. <https://docs.cupy.dev/en/stable/reference/generated/cupyx.scipy.sparse.linalg.svds.html>, 2025. Accessed: 2025-08-24.

Artem Riabinin, Egor Shulgin, Kaja Gruntkowska, and Peter Richtárik. Gluon: Making muon & scion great again!(bridging theory and practice of lmo-based optimizers for llms). *arXiv preprint arXiv:2505.13416*, 2025.

Ishaan Shah, Anthony M Polloreno, Karl Stratos, Philip Monk, Adarsh Chaluvavaraju, Andrew Hojel, Andrew Ma, Anil Thomas, Ashish Tanwer, Darsh J Shah, et al. Practical efficiency of muon for pretraining. *arXiv preprint arXiv:2505.02222*, 2025.

Hao-Jun Michael Shi, Shenyinying Tu, Yangyang Xu, and Wotao Yin. A primer on coordinate descent algorithms. *arXiv preprint arXiv:1610.00040*, 2016.

Egor Shulgin, Sultan AlRashed, Francesco Orabona, and Peter Richtárik. Beyond the ideal: Analyzing the inexact muon update, 2025. URL <https://arxiv.org/abs/2510.19933>.

Chongjie Si, Debng Zhang, and Wei Shen. Adamuon: Adaptive muon optimizer. *arXiv preprint arXiv:2507.11005*, 2025.

Kesheng Wuzand Horst Simonz. Thick-restart lanczos method for symmetric eigenvalue problems. 1998.

Nikhil Vyas, Depen Morwani, Rosie Zhao, Mujin Kwun, Itai Shapira, David Brandfonbrener, Lucas Janson, and Sham Kakade. Soap: Improving and stabilizing shampoo using adam, 2025. URL <https://arxiv.org/abs/2409.11321>.

Yao-Liang Yu. Arithmetic duality for norms, 2012. URL <https://cs.uwaterloo.ca/~y328yu/notes/normduality.pdf>.

A LMO FOR NEURAL NETWORKS

In a typical neural network, the objective function F depends on a set of weight matrices $\{\mathbf{W}_1, \mathbf{W}_2, \dots\}$. The optimization framework we have described is applied in a layer-wise fashion. At each iteration k , a stochastic gradient $g(\mathbf{X}^k, \xi^k)$ is computed using a mini-batch of data with the ξ^k noise via backpropagation. This yields a separate gradient component, \mathbf{G}_i^k , for each matrix \mathbf{X}_i . The LMO-based update rule is then applied to each matrix \mathbf{X}_i using its corresponding gradient component \mathbf{G}_i^k .

The update rule used in Muon optimizer is uSCG (Pethick et al., 2025c). In the most general case, which involves momentum, it can be written as

$$\begin{aligned}\mathbf{M}^k &= \alpha_k g(\mathbf{X}^k, \xi^k) + (1 - \alpha_k) \mathbf{M}^{k-1}, \\ \mathbf{X}^{k+1} &= \mathbf{X}^k + \gamma_k \text{LMO}(\mathbf{M}^k).\end{aligned}\tag{13}$$

B NORMS $\|\cdot\|_{F*}^\dagger$ AND $\|\cdot\|_{F2}^\dagger$

Based on the lemma, we immediately find $\|\cdot\|_{F*}^\dagger$, which is related to F-Muon update. Indeed, after setting $\beta = 1 - \alpha$ and remembering that for smooth and bounded cases we can use min instead of inf, we get

$$\|\mathbf{Y}\|_{F*}^\dagger = \min_{\mathbf{Z}} \min_t \{t, s.t. \|\mathbf{Z}\|_2 \leq \alpha t, \|\mathbf{Y} - \mathbf{Z}\|_F \leq (1 - \alpha)t\}\tag{14}$$

If $\alpha = 1$, then $\mathbf{Z} = \mathbf{Y}$, and we get $\|\mathbf{Y}\|_{F^*}^\dagger = \|\mathbf{Y}\|_2$. If $\alpha = 0$, then $\mathbf{Z} = 0$, and we get $\|\mathbf{Y}\|_{F^*}^\dagger = \|\mathbf{Y}\|_F$.

Similarly, we find $\|\cdot\|_{F2}^\dagger$, which is related to F-Neon update:

$$\|\mathbf{Y}\|_{F2}^\dagger = \min_{\mathbf{Z}} \min_t \{t, s.t. \|\mathbf{Z}\|_{\text{nuc}} \leq \alpha t, \|\mathbf{Y} - \mathbf{Z}\|_F \leq (1 - \alpha)t\} \quad (15)$$

If $\alpha = 1$, then $\mathbf{Z} = \mathbf{Y}$, and we get $\|\mathbf{Y}\|_{F2}^\dagger = \|\mathbf{Y}\|_{\text{nuc}}$. If $\alpha = 0$, then $\mathbf{Z} = 0$, and we get $\|\mathbf{Y}\|_{F2}^\dagger = \|\mathbf{Y}\|_F$.

Unfortunately, $\|\cdot\|_{F^*}^\dagger$ and $\|\cdot\|_{F2}^\dagger$ do not have a closed-form expression.

C VISUALIZATION OF DIFFERENT MATRIX NORMS

C.1 DUALS TO F* AND F2 NORMS

It follows from lemma 3 that the norm ball in $\|\cdot\|_{F^*}^\dagger$ is the Minkowski sum of the norm ball in $\alpha\|\cdot\|_{\text{nuc}}$ and $(1 - \alpha)\|\cdot\|_F$ and the norm ball in $\|\cdot\|_{F2}^\dagger$ is the Minkowski sum of the norm ball in $\alpha\|\cdot\|_2$ and $(1 - \alpha)\|\cdot\|_F$.

In Fig. fig. 5 we plot these norms. On x-axis and y-axis, there are singular values σ_1, σ_2 respectively of a matrix from $\mathbb{R}^{m \times n}$ with $\min\{m, n\} = 2$.

C.2 THE KY FAN NORM AND ITS DUAL

1-balls in l_∞ , l_1 and l_2 norms are well-known from textbooks. But what about the Ky Fan k -norm? How can it be represented?

To showcase the complex structure of the Ky Fan k -norm and its dual, we suggest the illustrations fig. 6 with the ball in the Ky Fan 2-norm in fig. 6a and its dual in fig. 6b. On x-, y-, and z-axes, there are singular values σ_1, σ_2 , and σ_3 respectively of a matrix from $\mathbb{R}^{m \times n}$ with $\min\{m, n\} = 3$. In this particular case, we do not sort the singular values. In the proposed representation, we actually plot balls in the Top-2 norm $\max\{|x| + |y|, |x| + |z|, |y| + |z|\}$ and its dual norm $\max\{\max(|x|, |y|, |z|), \frac{1}{2}(|x| + |y| + |z|)\}$. The resulting balls are much more complex than balls in l_∞ , l_1 and l_2 norms.

In fact, those balls can be described easier if we use the results from Yu (2012). The Ky Fan 2-norm ball is an intersection of three l_1 balls in (x, y) , (x, z) , and (y, z) spaces. The 1-ball in the dual Ky Fan 2-norm is an intersection of 1-ball the in l_∞ norm and $\frac{1}{2}$ -ball in the l_1 norm.

D MORE DATA FOR LINEAR LEAST SQUARES

E TECHNICAL DETAILS OF THE EXPERIMENTS

We compared TRLand with other methods in Google Colab. We used RTX A4000 for CIFAR airbench.

Method	lr	momentum	Iterations to 0.01 loss
NSGD	0.25	0.9	350
SignSGD	0.055 - 0.01	0.95	700
Muon	0.025	0.5	290
F-Muon	0.035	0.5	320
S-Muon	0.035	0.8	270

Table 4: Tuning lrs and momentum coefficients

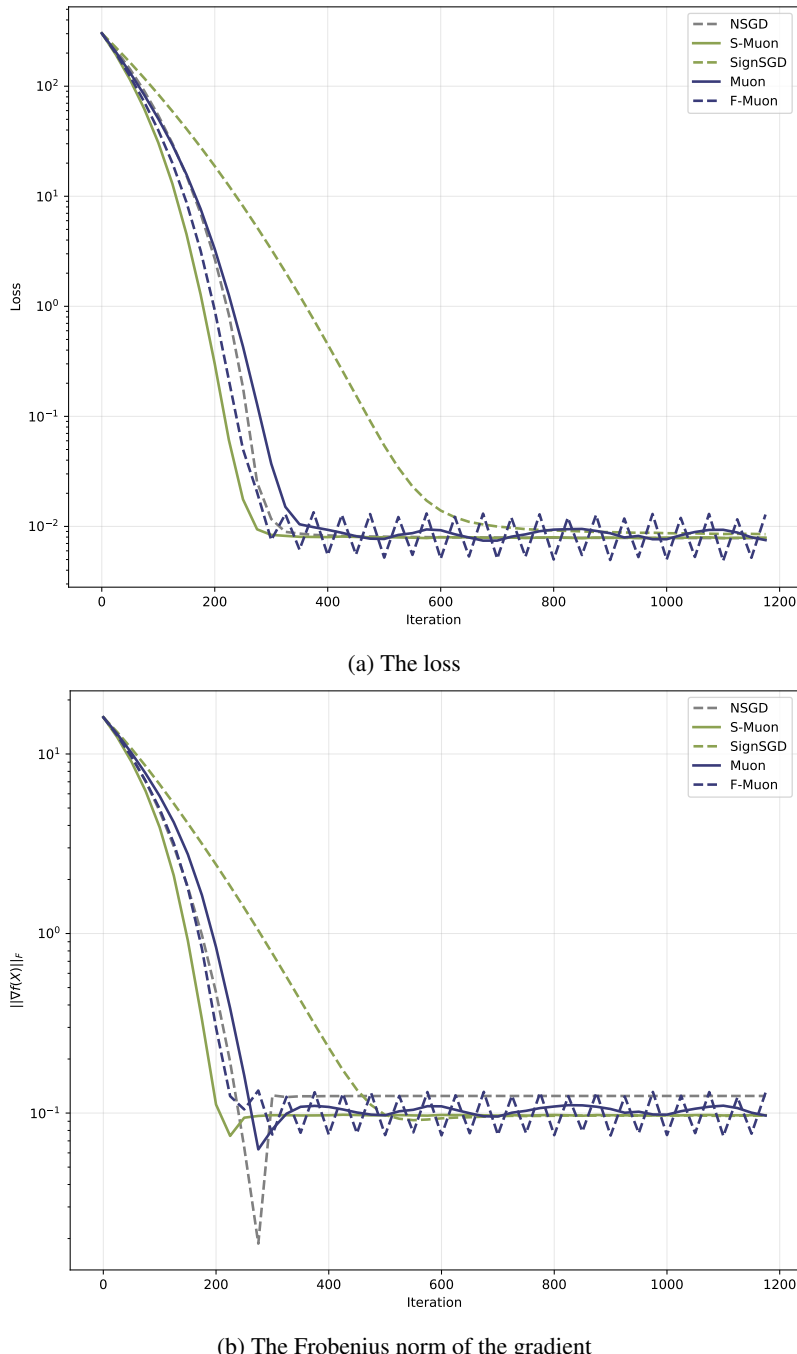


Figure 1: Linear least squares problem for a 500x500 matrix

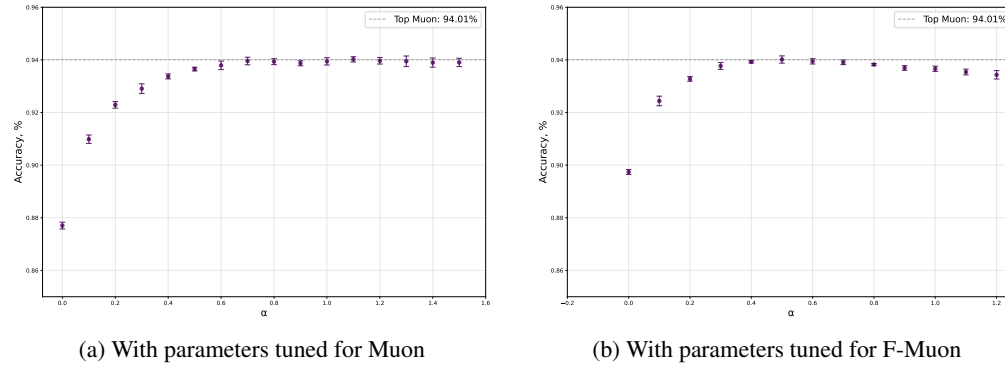


Figure 2: Mean validation accuracies for F-Muon with different α

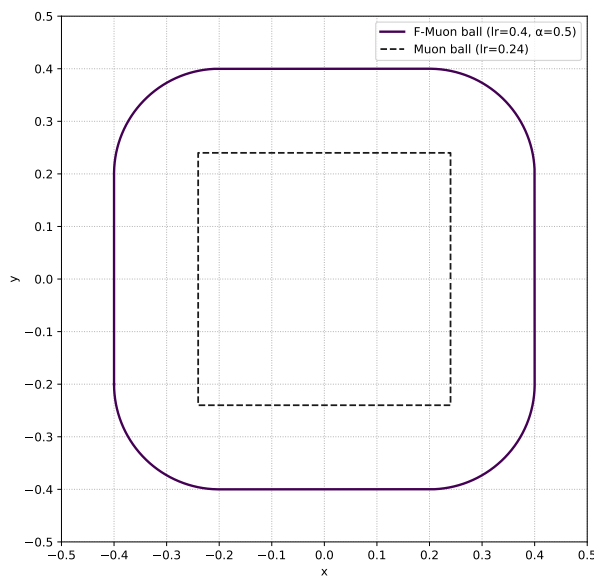


Figure 3: Visualization of the LMO balls for Muon and F-Muon.

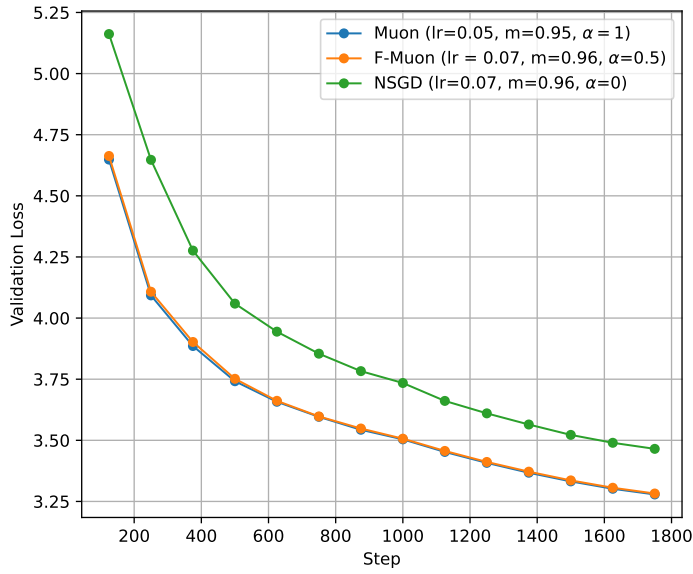


Figure 4: The validation loss for NanoGPT

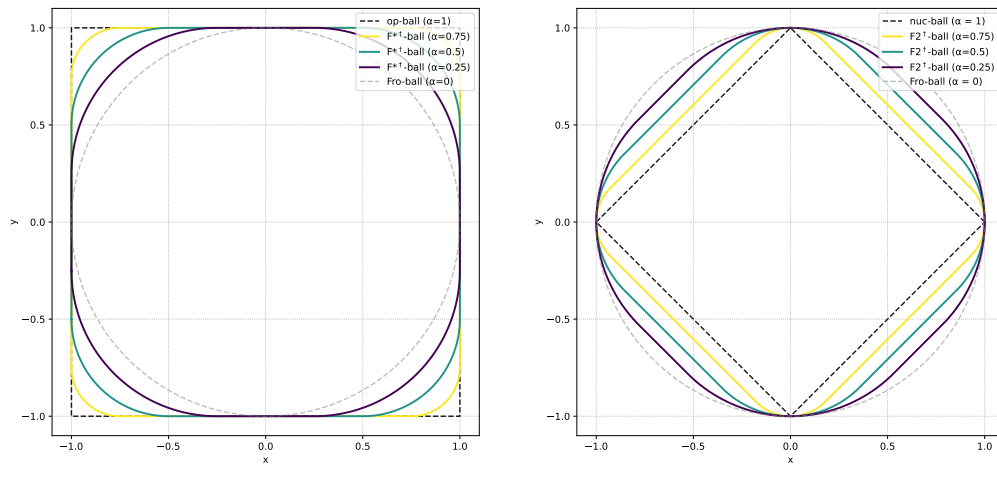


Figure 5: Balls in the duals to F^* and F_2 norms for different α

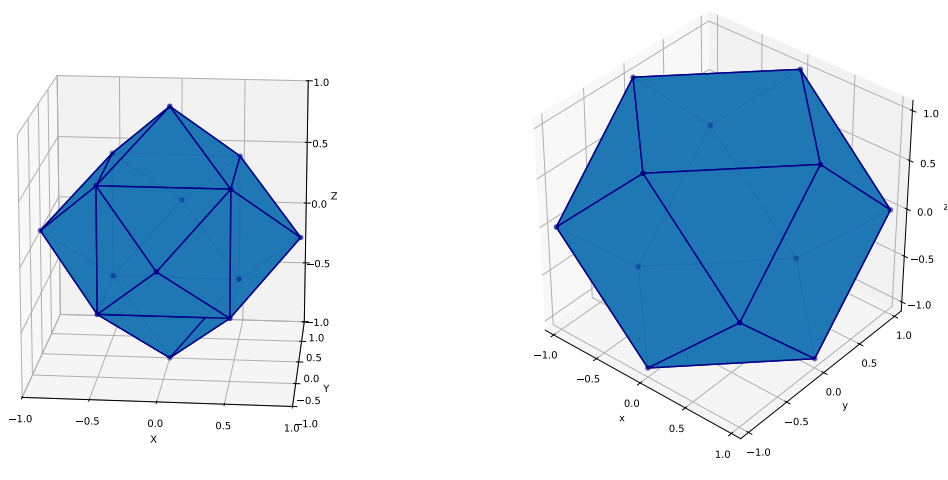


Figure 6: Ky Fan 2-norm and its dual

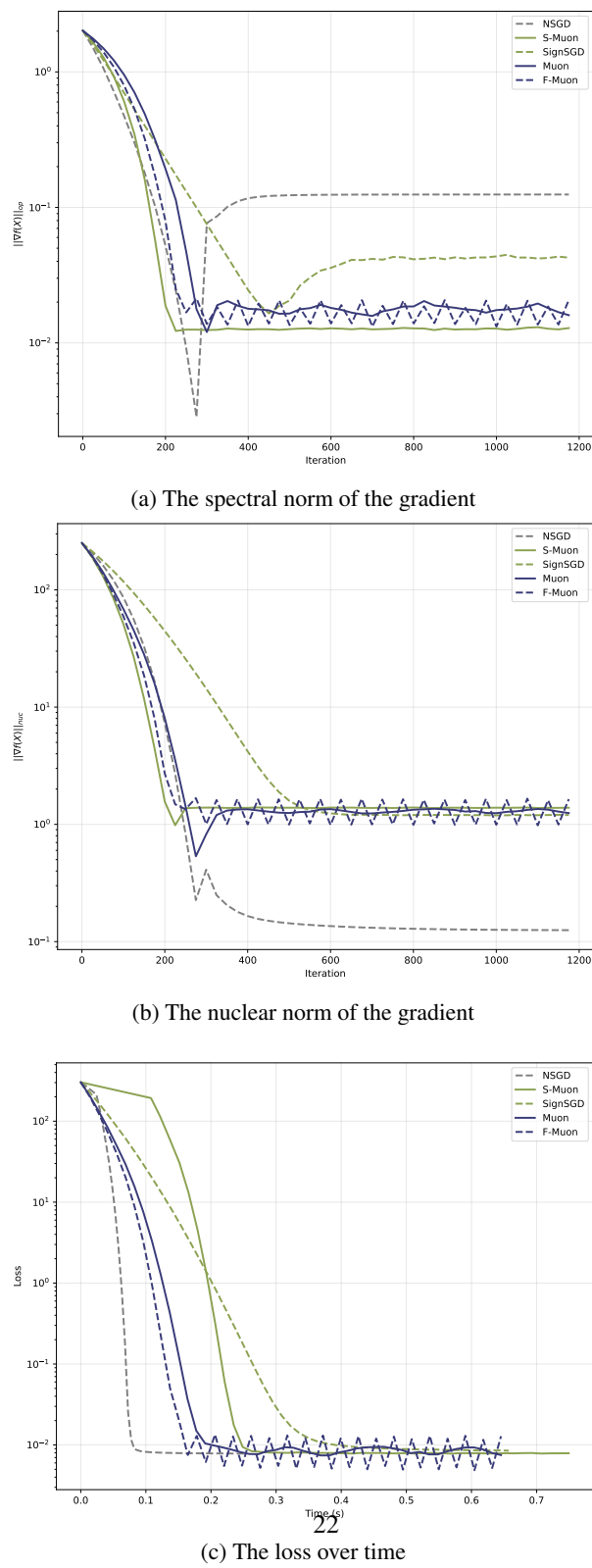


Figure 7: More images for Linear least squares problem for a 500x500 matrix